Development of an X-band SAR ship detectability model

Analysis of TerraSAR-X ocean imagery

Paris W. Vachon, Ryan English, Nicholas Sandirasegaram, John Wolfe

This Technical Memorandum is the Final Report for TerraSAR-X Announcement of Opportunity Project COA308.

Defence R&D Canada – Ottawa

Technical Memorandum
DRDC Ottawa TM 2013-120
December 2013

Principal Author

Original signed by Paris W. Vachon

Paris W. Vachon

Defence Scientist

Approved by

Original signed by Maj. Catherine Marchetti

Maj. Catherine Marchetti

A/Head, Space & ISR Applications

Approved for release by

Original signed by Chris McMillan

Chris McMillan

Chair, Document Review Panel

Abstract

A C-band SAR Ship Detectability Performance Tool has been extended to X-band synthetic aperture radar (SAR) by analyzing TerraSAR-X ocean imagery. First, a database of validated X-band SAR ship signatures was developed using coastal-received Automatic Identification System (AIS) data over the Strait of Gibraltar. The database was used to derive a semi-empirical model for the ship radar cross section (RCS) and its variability. Second, X-band SAR imagery of meteorological buoys has provided a set of X-band ocean backscatter measurements for known wind conditions. These measurements have been used to validate a model that relates X-band ocean backscatter to wind speed. The upgraded X-band SAR Ship Detectability Performance Tool can be used to predict the ship detection performance of existing and future X-band SAR missions, which could include the follow-on to the RADARSAT Constellation Mission.

Résumé

Grâce à l'analyse d'images océaniques produites par TerraSAR-X, on a adapté aux radars à synthèse d'ouverture (RSO) en bande X un outil utilisé pour prévoir le rendement en matière de détection de navires de RSO en bande C. Premièrement, on a établi une base de signatures validées relatives à des navires détectés par un ou des RSO en bande X en utilisant des données recueillies au-dessus du détroit de Gibraltar et captées par un ou des systèmes d'identification automatiques côtiers. La base de signatures a ensuite été utilisée pour produire un modèle semi-empirique de la section efficace en radar (radar cross section – RCS) de navires, ainsi que de la variabilité de la RCS. Deuxièmement, on s'est servi d'images de RSO en bande X représentant des bouées météorologiques pour établir un ensemble de mesures de rétrodiffusion océaniques en bande X relatives aux vents, mesures qui ont ensuite été utilisées pour valider un modèle de comparaison de la rétrodiffusion océanique en bande X et des vents. L'outil amélioré ainsi obtenu peut servir à prévoir le rendement en matière de détection de missions en cours et à venir de RSO en bande X, dont celle devant suivre la mission de Constellation RADARSAT.

This page intentionally left blank.

Executive summary

Development of an X-band SAR ship detectability model: Analysis of TerraSAR-X ocean imagery

Paris W. Vachon; Ryan English; Nicholas Sandirasegaram; John Wolfe; DRDC Ottawa TM 2013-120; Defence R&D Canada – Ottawa; December 2013.

Introduction: A C-band synthetic aperture radar (SAR) Ship Detectability Performance Tool has been extended to X-band SAR based upon analysis of TerraSAR-X ocean imagery.

TerraSAR-X imagery was acquired in a variety of modes concurrently with coastal-received Automatic Identification System (AIS) data over the Strait of Gibraltar, a high-density shipping region. The data have been used to develop a database of validated ship signatures at X-band. The database was used to derive a semi-empirical model for X-band ship radar cross section (RCS) and its variability.

Furthermore, TerraSAR-X imagery acquired over operational meteorological buoys located off the east coast of Canada have provided a set of X-band ocean backscatter measurements for known wind conditions. These measurements have been used to validate an X-band geophysical model function referred to as XMOD that describes the relationship between X-band ocean backscatter and ocean surface wind speed.

Results: It was found that the X-band co-polarization (co-pol) ship RCS is about 13.6 dB larger than X-band cross-polarization (cross-pol) ship RCS. Furthermore, compared with previous C-band results, X-band co-pol ship RCS is about 2.6 dB larger than C-band co-pol ship RCS, and X-band cross-pol ship RCS is about 0.8 dB larger than C-band cross-pol ship RCS.

XMOD was successfully validated with RMS errors in comparing the SAR-derived and *in situ*-observed wind speeds of less than 1.2 m/s, for both VV and HH polarization data. The cross-pol observations were too close to the instrument noise floor to provide any useful information.

The upgraded SAR Ship Detectability Performance Tool was used to compare the minimum detectable ship length for X-band and C-band SAR, all else held equal. It was observed that X-band performs as well as or better than C-band, presumably because the ship RCS is larger at X-band than at C-band.

Significance: The upgraded X-band SAR Ship Detectability Performance Tool can be used to predict the ship detection performance of existing and future X-band SAR missions, which could include the follow-on to the RADARSAT Constellation Mission.

Sommaire

Development of an X-band SAR ship detectability model: Analysis of TerraSAR-X ocean imagery

Paris W. Vachon; Ryan English; Nicholas Sandirasegaram; John Wolfe ; DRDC Ottawa TM 2013-120 ; R & D pour la défense Canada – Ottawa; décembre 2013.

Introduction : Grâce à l'analyse d'images océaniques produites par TerraSAR-X, on a adapté aux radars à synthèse d'ouverture (RSO) en bande X un outil utilisé pour prévoir le rendement en matière de détection de navires de RSO en bande C.

Les images de TerraSAR-X ont été produites selon divers modes et en parallèle avec l'acquisition de données recueilles au-dessus du détroit de Gibraltar, où le trafic maritime est important, et captées par un ou des systèmes d'identification automatiques côtiers. Les données ont servi à établir une base de signatures validées rattachées à des navires détectés par un ou des RSO en bande X. La base de signatures a été utilisée pour produire un modèle semi-empirique de la section efficace en radar (radar cross section – RCS) de navires, ainsi que de la variabilité de la RCS.

Par ailleurs, on a utilisé des images de TerraSAR-X représentant des bouées météorologiques situées au large de la côte Est du Canada pour établir un ensemble de mesures de rétrodiffusion océaniques en bande X relatives aux vents observés, mesures qui ont ensuite été utilisées pour valider une fonction de modèle géophysique en bande X baptisée « XMOD », qui sert à décrire la relation entre la rétrodiffusion océanique en bande X et la vitesse des vents soufflant à la surface de l'océan.

Résultats : On a découvert que la RCS de copolarisation en bande X d'un navire est supérieur d'environ 13,6 dB à sa RCS de polarisation croisée en bande X. De plus, en la comparant à des résultats en bande X antérieurs, on a constaté qu'elle est supérieure de quelque 2,6 dB à la RCS de copolarisation en bande C et d'approximativement 0,8 dB à la RCS de polarisation croisée en bande C.

Le modèle XMOD a été validé avec succès, celui-ci présentant des erreurs quadratiques moyennes inférieures à 1,2 m/s, tant pour des données de polarisation VV que des données de polarisation HH, pendant la comparaison de vitesses du vent dérivées de données de RSO et de vitesses observées in situ; les observations de polarisation croisée n'ont fourni aucune information utile, car elles s'approchaient trop du seuil de bruit du ou des instruments.

L'outil amélioré obtenu peut servir à comparer la longueur minimale d'un navire détectable par un RSO en bandes X et C, si aucun autre élément ne change. On a observé que le rendement en bande X est équivalent ou supérieur à celui en bande C, ce qui serait attribuable à une RCS de navire supérieure en bande X qu'en bande C.

Importance : L'outil amélioré peut servir à prévoir le rendement en matière de détection de missions en cours et à venir de RSO en bande X, dont celle devant suivre la mission de Constellation RADARSAT.

Table of contents

List of figures

List of tables

This page intentionally left blank.

1 Introduction

In this project, a C-band synthetic aperture radar (SAR) Ship Detectability Performance Tool [5] was extended to X-band by analyzing TerraSAR-X ocean imagery. A new model for X-band ship radar cross-section (RCS) and its variability was developed, and a model that relates ocean backscatter to wind speed was validated.

C-band models for RCS ship and its variability that were developed using RADARSAT-1 SAR imagery [2], [3] and Envisat ASAR alternating polarization mode imagery [4], were extended to X-band. To achieve this, TerraSAR-X SAR imagery (see, http://www.dlr.de/dlr/en/desktopdefault.aspx/tabid-10422/#gallery/9106/ or http://www.astrium-geo.com/terrasar-x/) were acquired in a variety of modes concurrently with coastal-received Automatic Identification System (AIS) data over the Strait of Gibraltar, a high-density shipping region, allowing the creation of a database of ship signatures at X-band for which we have high confidence in the identity and details about each ship.

AIS (see, *e.g.*, http://navcen.uscg.gov/?pageName=AISmain) is a VHF-based ship-to-ship transponder system intended for collision avoidance and vessel traffic management that is mandated for commercial shipping, particularly on international voyages, but is also in heavy domestic use in many locales. AIS messages include ship identification, location, velocity, type, cargo, *etc.* and may be received and decoded using a shore-based VHF antenna and receiver. AIS has become an important maritime intelligence, surveillance, and reconnaissance (ISR) asset.

Ship signature databases comprised of thousands of ships have already been developed for C-band SAR imagery using shored-based AIS data from the Maritime Safety and Security Information System (MSSIS) (see, https://mssis.volpe.dot.gov/) [5]. The new X-band ship signature database was used to derive semi-empirical models for the ship RCS and its variability and to derive ship signature metrics, such as the signature length, which may be used for automatic target recognition. These models can also be used to reduce false alarms in operational ship detection systems.

A second component of the project was to evaluate the state of ocean backscatter modelling at X-band [1]. To this end, a second TerraSAR-X data set was acquired over operational meteorological buoys located off the east coast of Canada. This provided a set of X-band backscatter measurements for known wind conditions. Although the data set is too small to permit the development of a new X-band wind retrieval model function, it is sufficient to evaluate the performance of existing X-band model functions.

This report is organized as follows: Section 2 describes the ship signature analysis; Section 3 describes the ocean backscatter analysis; Section 4 presents results from the upgraded X-band SAR Ship Detectability Tool; and Section 5 presents the conclusions of the project.

2 Ship detection

2.1 Data set

Thirty-three TerraSAR-X Images of the Gibraltar region were acquired in a variety of modes and polarizations along with contemporaneous AIS data obtained via MSSIS. The AIS static data (*i.e.*, ship identification and dimensions) were verified through an authoritative Internet Ships Register (ISR) (see, http://www.ships-register.com/). In particular, the validated ship length (VSL) is used as the ship length reference for each ship in the database. The Length Overall field in the ISR database is referred to as validated ship length (VSL) in this report.

The AIS data were cast into the frame of reference of the SAR image by interpolating the AIS-reported ship positions to the time of the SAR pass (the AIS-projected position), then azimuth shifting the AIS-projected position to account for the Doppler shift associated with moving targets using the AIS-derived ship velocity and the SAR acquisition geometry (the AIS-predicted position) [3]. An example is shown in Figure 1.

A search of each TerraSAR-X image was carried out within a 400 m radius of the AIS-predicted positions to find candidate ship signatures. For the TerraSAR-X data, the distance between the AIS-predicted location and the actual SAR ship signature location was on the order of 50 m, leading to virtual certainty in the association of shore-based AIS data with a specific ship signature. For each ship, the total RCS, the estimated ship length (ESL), and other parameters were derived from the ship signature using the VuSAR tool [2]. The HH and VV data were combined as co-polarization (co-pol), while the HV and VH data were combined as cross-polarization (cross-pol). This resulted in a database comprised of 364 validated ships in X-band co-pol and 202 validated ships in X-band cross-pol.

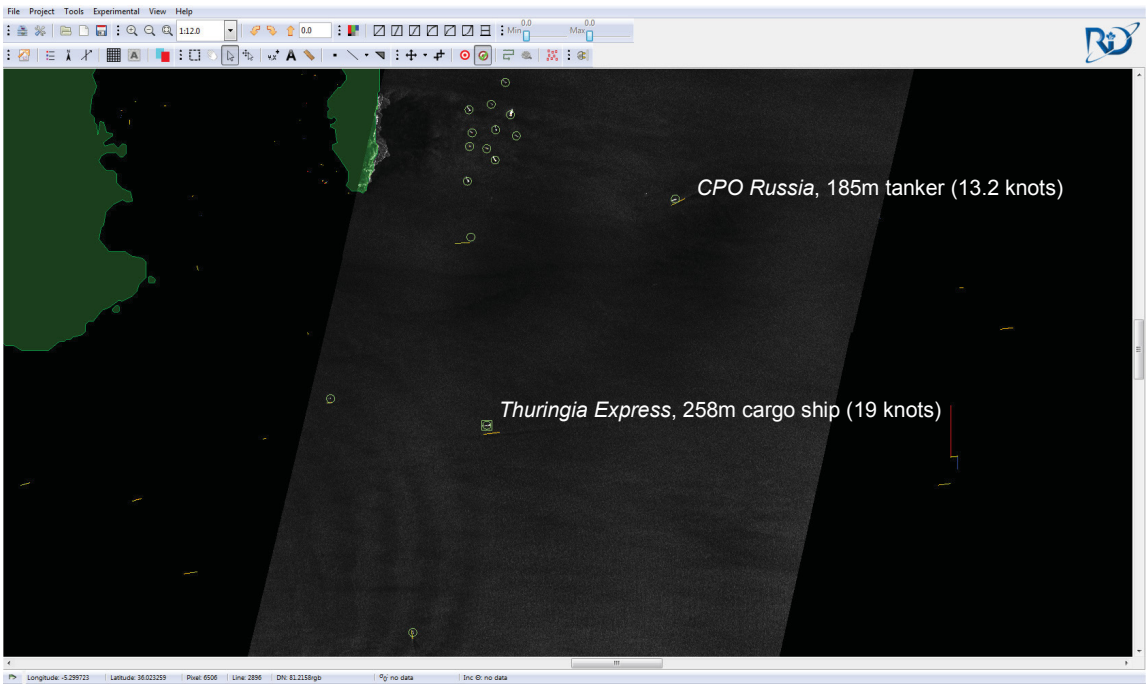

Figure 1: HH stripmap mode TerraSAR-X image of the Straits of Gibraltar acquired 2009-11-02, showing anchored and moving vessel signatures with several well-defined wakes visible. MSSIS AIS data was used to dead-reckon forward (red), backward (blue), and interpolate (yellow). Doppler shifting to the AIS-predicted positions (green circles) locates the SAR signatures of the vessels at the image acquisition time. (Image (c) DLR 2009.).

2.2 Ship RCS and its variability

Following previous work at C-band [5], the X-band ship RCS in square-metres is assumed to be parameterized by the ship-length-squared, and is given by:

$$\sigma = aAL^2 , \tag{1}$$

where L is the VSL in metres and A and a are polarization-dependent model coefficients. Choosing $a = 1$ gives the nominal form of the model. Choosing $a = a_{\text{min-VSL}}$ gives the fifth-percentile (say) of ship RCS while choosing $a = a_{\text{max-VSL}}$ gives the ninety-fifth percentile (say) of ship RCS. That is, the RCS range between $a_{\text{min-VSL}}$ and $a_{\text{max-VSL}}$ would encompass 90% of the ships considered, provided the ship length is known. This approach captures ship RCS variability that could arise from ship type, ship orientation, incidence angle, *etc*.

The X-band ship RCS model coefficients were estimated by plotting the cumulative probability density function of the observed X-band ship RCS values as a function of the model parameter a, as shown in Figure 2. The X-band ship RCS is plotted as a function of VSL in Figure 3. The X-band ship RCS model coefficients are provided in Table 1.

From the table, it is apparent that co-pol X-band ship RCS is about 13.6 dB larger than cross-pol X-band ship RCS. Furthermore, comparing these values with previous C-band results [5], X-band co-pol ship RCS is about 2.6 dB larger than C-band co-pol ship RCS, and X-band cross-pol ship RCS is about 0.8 dB larger than C-band cross-pol ship RCS.

a) b)

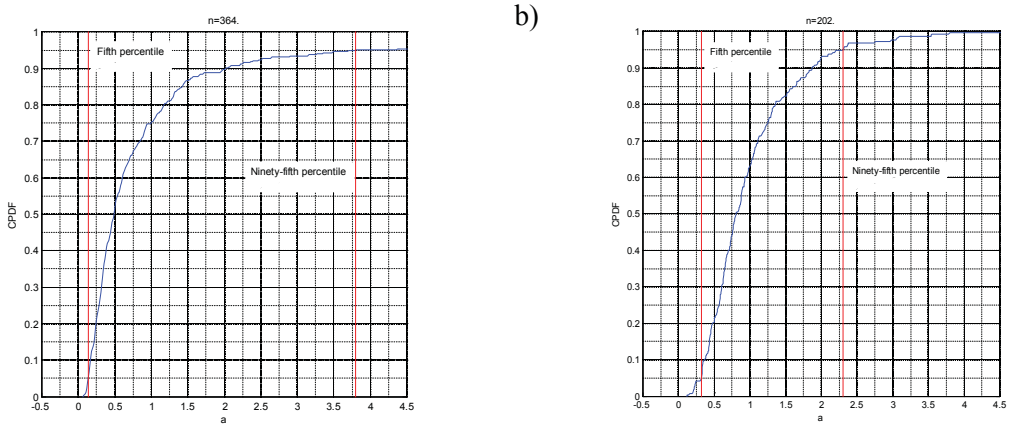

Figure 2: X-band ship RCS cumulative probability density function (CPDF) as a function of the model coefficient a for: a) co-pol; and b) cross-pol.

a) b)

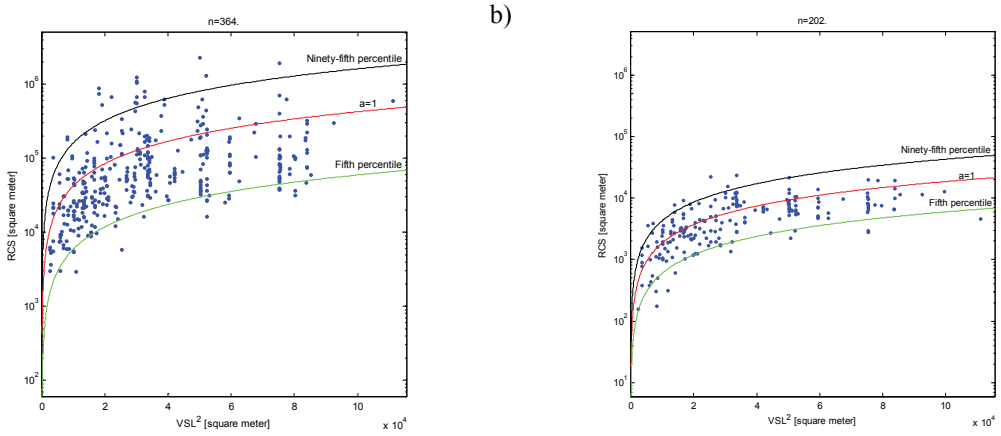

Figure 3: X-band ship RCS as a function of VSL-squared for: a) co-pol; and b) cross-pol.

Table 1: X-band ship RCS model coefficients that encompass 90 % of the observed ships, using Equation (1) with L = VSL.

Polarization	A	$a_{\text{min-VSL}}$	$a_{\text{max-VSL}}$
co-pol	4.26	0.140	3.80
cross-pol	0.186	0.321	2.31

2.3 Ship length estimation

Having ESL and VSL for a significant number of ships, the relationship between the two lengths and comparative statistics can be derived. The ship length error may be defined as:

$$\Delta L = \mathrm{ESL} - \mathrm{VSL} = \mathrm{ESL} - L\,, \tag{2}$$

and the normalized ship length error may be defined as:

$$\mathrm{NE} = \frac{\Delta L}{L}. \tag{3}$$

These parameters have been compiled in

Table 2, which provides the two polarization cases considered, the number of ships in each case, the minimum (Min), maximum (Max), mean (Mean), and standard deviated (STD) of VSL, the minimum and maximum of ESL, the root-mean-square (RMS) of ΔL, and the mean and standard deviation of NE.

The ships considered were all fairly large in size since only vessels larger than 300 tons are mandated to carry AIS equipment. Vessels ranged from 49 m to 333 m in length. The mean vessel length was roughly 171 m with a standard deviation of 64 m.

To better understand the distribution of ESL and VSL, scatter plots of each case in

Table 2 were generated, along with histograms of NE (see Figure 4 and Figure 5). A 50% error in ESL describes most of the observed variability. ESL and VSL are quite well-correlated, with the RMS of NE being 85 m for co-pol and 54 m for cross-pol. The occurrence of differences in these parameters may be attributed in part to the performance of the ship length estimation algorithm, but likely arises from azimuth smearing of ship signatures due to target motion (leading to overestimates of ship length), and obliteration of portions of the ship signature due to high background clutter levels (leading to underestimates of ship length). In general, ship length estimation performs better at cross-pol.

The NE parameter has a positive bias of about 13% for co-pol and 12% for cross-pol. There are more overestimates of ship length than underestimates of ship length, suggesting that azimuth smearing of ship signatures is a bigger problem than high clutter levels obliterating portions of the ship signature for this database. ESL values ranged from 4 m (roughly twice the image resolution) to 972 m, neither of which are realistic ship lengths.

To encompass a certain fraction of the observed ships, defined as η (*e.g.*, η = 0.9 for 90%), the value of NE for $p = 100*(0.5 - \eta/2)$ and $q = 100*(0.5 + \eta/2)$ (*i.e.*, p is the 5$^{\text{th}}$ percentile and q is

the 95th percentile for η = 0.9) were estimated for both co-pol and cross-pol. Percentile values corresponding to η = 0.6, 0.8, and 0.9 are compiled in Table 3.

Table 2: Statistics of VSL and ESL.

Polarization	***# of ships***	**VSL [*m*]**				**ESL [*m*]**		ΔL **[*m*]**	**NE**	
		Min	***Max***	***Mean***	***STD***	***Min***	***Max***	***RMS***	***Mean***	***STD***
co-pol	364	49	333	171	64	4	972	85	0.129	0.830
cross-pol	202	49	333	174	64	5	543	54	0.121	0.570

Table 3: Distribution of NE: a) η = 0.9 (5th and 95th percentiles); b) η = 0.8 (10th and 90th percentiles); and c) η = 0.6 (20th and 80th percentiles).

a)

Polarization	**NE**		A	$a_{\min\_VSL}$	$a_{\max\_VSL}$	$a_{\min\_ESL}$	$a_{\max\_ESL}$
	<5th	***>95th***					
co-pol	−0.408	1.27	4.26	0.140	3.80	0.0491	19.6
cross-pol	−0.172	0.851	0.186	0.321	2.32	0.220	7.90

b)

Polarization	**NE**		A	$a_{\min\_VSL}$	$a_{\max\_VSL}$	$a_{\min\_ESL}$	$a_{\max\_ESL}$
	<10th	***>90th***					
co-pol	−0.201	0.194	4.26	0.174	2.03	0.111	2.89
cross-pol	−0.140	0.247	0.186	0.358	1.87	0.265	2.91

c)

Polarization	**NE**		A	$a_{\min\_VSL}$	$a_{\max\_VSL}$	$a_{\min\_ESL}$	$a_{\max\_ESL}$
	<20th	***>80th***					
co-pol	−0.109	0.0750	4.26	0.242	1.18	0.193	1.36
cross-pol	−0.0801	0.0812	0.186	0.474	1.35	0.401	1.58

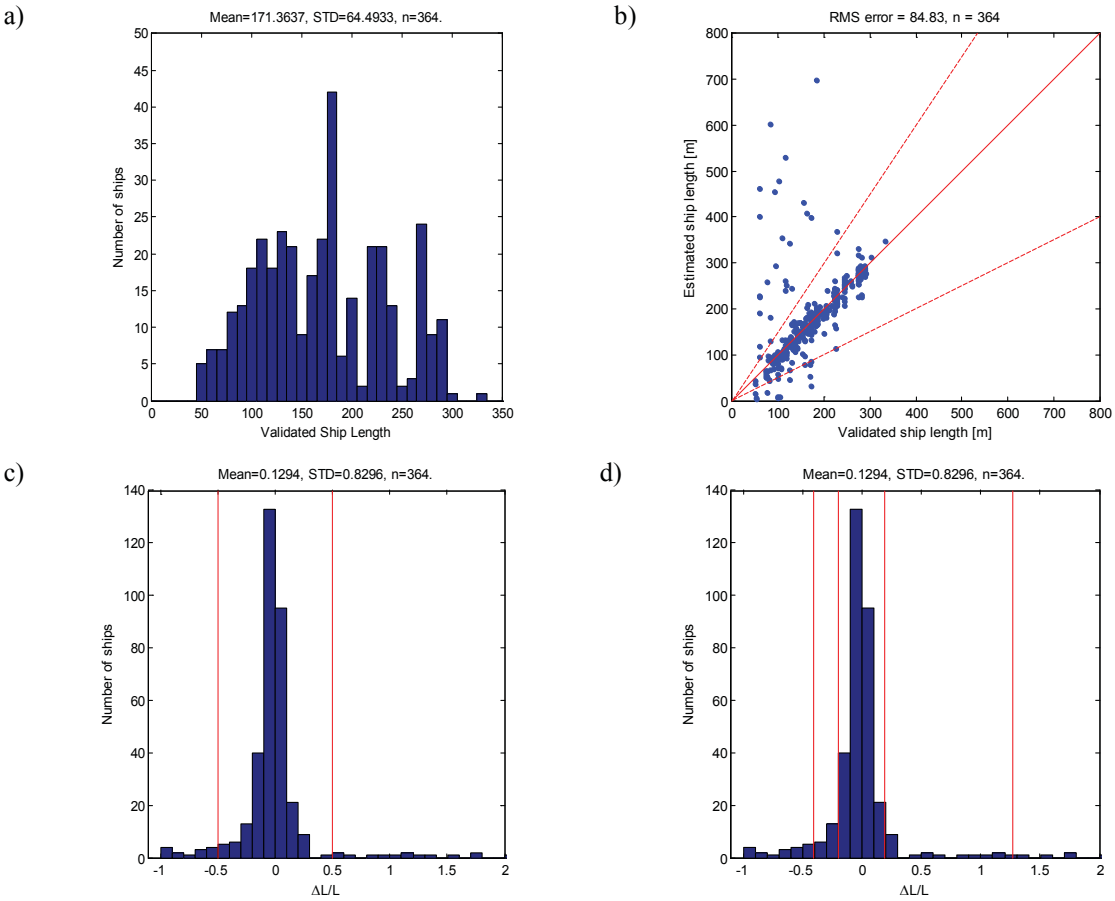

Figure 4: TerraSAR-X co-pol. a) VSL Histogram; b) ESL and VSL scatter plot, dashed lines are NE > 50 % (upper), NE < −50 % (lower); c) NE histogram, solid lines are NE > 50 % (right), NE < −50 % (left); d) NE histogram, solid lines are 5th, 10th, 90th, and 95th percentiles (left-to-right).

The X-band ship RCS model depends upon knowledge of the ship length *L*. In a practical ship detection system, the ship length may not be known, but could be estimated directly from the image (*i.e.*, ESL) and, therefore, would also have inherent errors. Based upon errors in ship length estimation alone, the lower and upper bound RCS limits of Equation (1) may be derived from the percentile values that are provided in

Table 3. Of course, these percentile values apply to an ESL estimated from high resolution TerraSAR-X beam modes. It is expected that the errors in estimating ship length would be higher for coarser resolution modes (*e.g.*, ScanSAR modes). Nevertheless, these values do allow an assessment of the impact of ship length estimation errors on the ship RCS.

The RCS scale factors were estimated as (1 + p-th percentile)-squared and (1 + q-th percentile)-squared, resulting in upper and lower bound RCS multipliers that we designate as $a_{\min\_ESL}$ and $a_{\max\_ESL}$ These values are tabulated in Table 3 for various values of η. That is, the X-band ship RCS model of Table 3 is is an updated version of the model in Table 1 that accounts for using ESL rather than VSL.

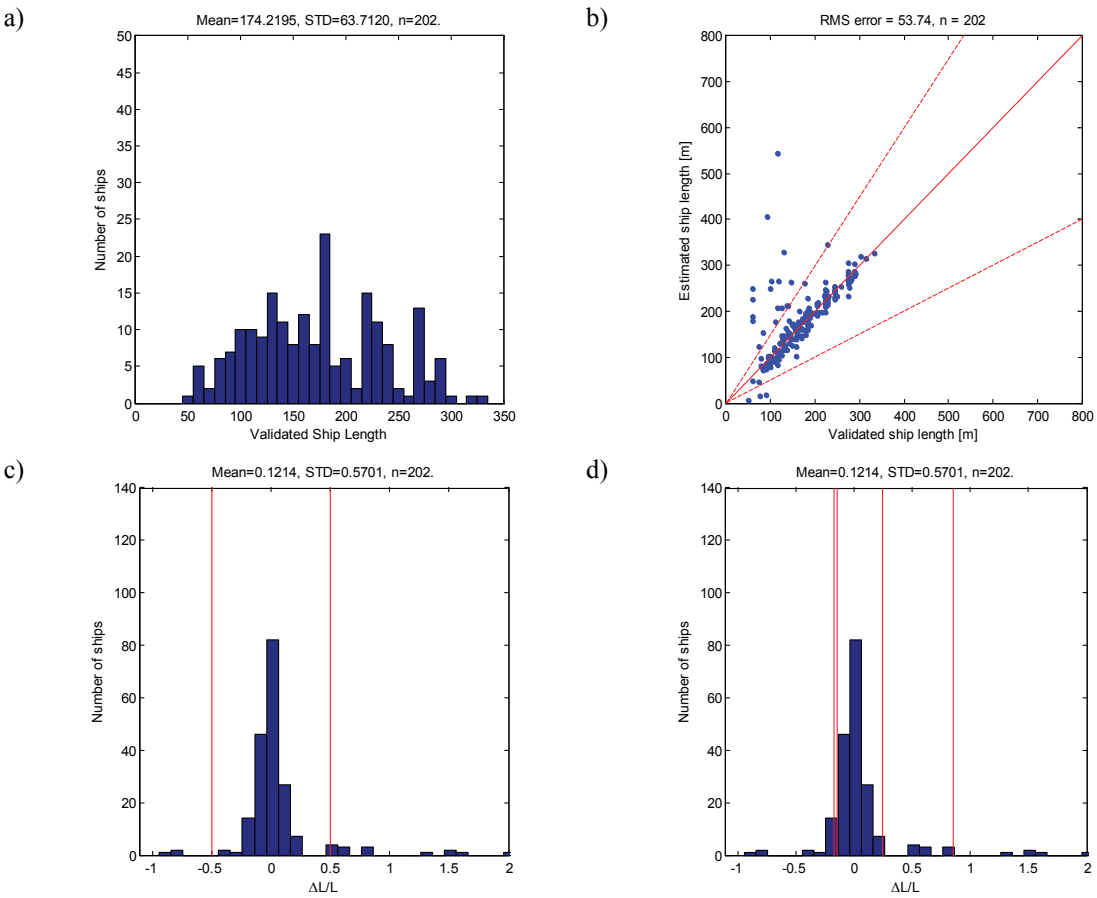

Figure 5: TerraSAR-X cross-pol. a) VSL Histogram; b) ESL and VSL scatter plot, dashed lines are NE > 50 % (upper), NE < −50 % (lower); c) NE histogram, solid lines are NE > 50 % (right), NE < −50 % (left); d) NE histogram, solid lines are 5th, 10th, 90th, and 95th percentiles (left-to-right).

3 Ocean backscatter

3.1 Data set

Twenty-four TerraSAR-X stripmap mode images were acquired of operational Canadian meteorological buoys that are maintained by Environment Canada and Fisheries and Oceans Canada (see Figure 6). The buoys provide contemporaneous measurements of wind speed and direction; an example image is shown in Figure 7. While this volume of data is inadequate to tune a new X-band ocean backscatter model, it is sufficient to validate a recently-published X-band VV polarization Geophysical Model Function (GMF) that is referred to as XMOD [1]. X-band HH polarization can be modelled by using XMOD and a co-polarization ratio [1]. In Figure 8, XMOD is compared with a C-band GMF. It is apparent that the ocean backscatter is generally higher at X-band than at C-band and that there is less contrast between upwind (φ = 0°) and downwind (φ = 90°) wind aspect angles at X-band than at C-band.

In each case, the buoys lay within the image footprint, and the SAR acquisition time was within 30 minutes of the buoy measurement. The single-look SAR image data were spatially averaged over a 512 by 512 pixel analysis chip centered on the buoy location. For the products used, this corresponds to a chip size of 460 m in range by 1229 m in azimuth. The ocean backscatter, σ°, the instrument noise floor, $\sigma^\circ_{\mathrm{NE}}$, and a K-distribution order parameter, ν, based on the mean and variance of the image intensity, were estimated for each image chip. The buoy wind speed was corrected to the equivalent neutral stability wind speed at a 10 m height above the ocean surface (*i.e.*, $U^{10}_{\mathrm{neutral}}$) using the observed air-sea temperature difference and the known anemometer height. This resulted in 15 observations for X-band VV polarization, 14 observations for X-band HH polarization, 6 observations for X-band HV polarization, and 7 observations for X-band VH polarization for a total of 42 observations. The maximum wind speed in the data set is just under 12 m/s. The wind data are tabulated in Table 4, which is found in Annex A.

Figure 9 shows a plot of the estimated K-distribution order parameters. The values range from <2 (heterogeneous clutter) to large values that were limited to a maximum of 100 (homogenous clutter). Most of the cross-pol observations had large order parameters.

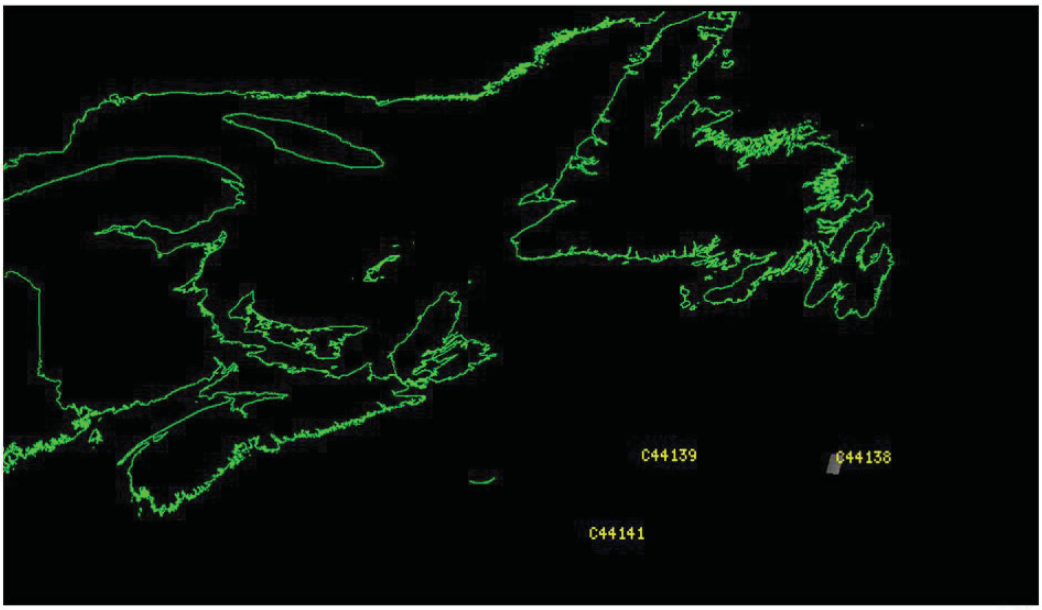

Figure 6: Atlantic buoy locations considered.

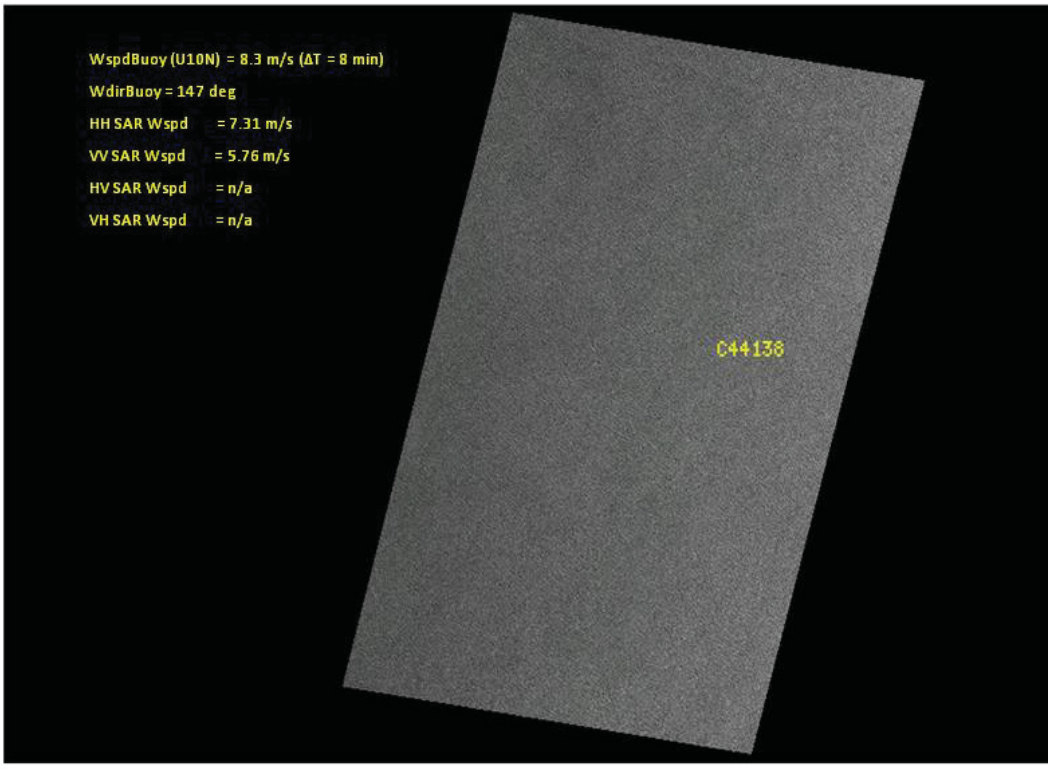

Figure 7: HH stripmap TerraSAR-X image of the Atlantic Ocean south of St. John's acquired 2011-08-05, showing the location of a Canadian operational buoy. (Image © DLR 2011.)

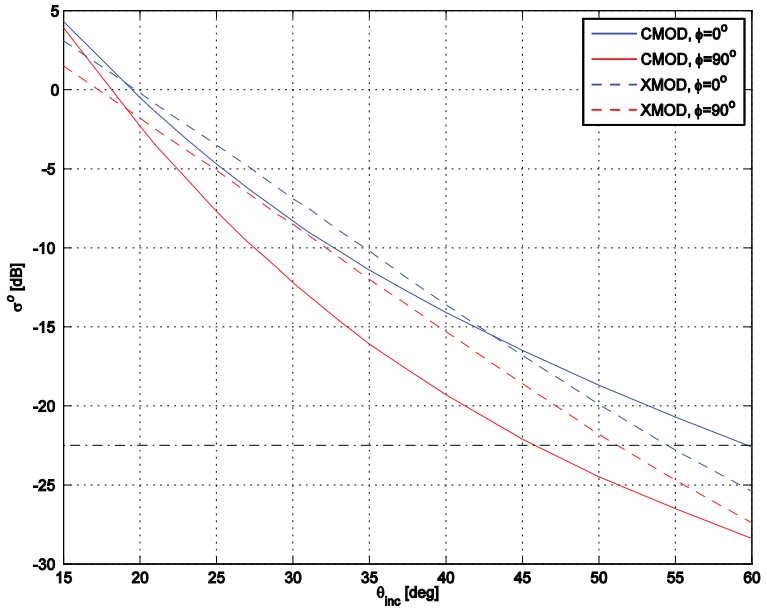

Figure 8: Comparison of X-band (XMOD) and C-band (CMOD) backscatter as a function of incidence angle. The horizontal line represents a nominal noise floor of −22.5 dB.

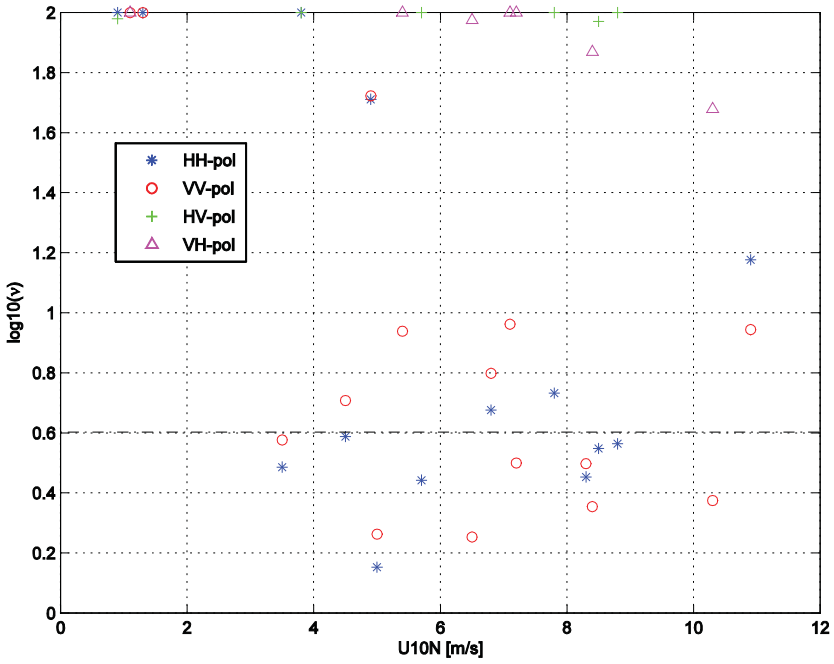

Figure 9: K-distribution order parameter, ν, as estimated from the TerraSAR-X analysis chips. The horizontal line corresponds to ν = 4.

3.2 Backscatter comparison with XMOD

Figure 10 shows plots of X-band co-pol and cross-pol backscatter (*i.e.*, sigma naught or σ°) as a function of incidence angle (θ_{inc}). Also plotted is the instrument noise floor (*i.e.*, the noise-equivalent sigma naught or σ°_{NE}), which was estimated from the TerraSAR-X product metadata. The X-band co-pol backscatter data show the expected downward trend in backscatter with increasing incidence angle. Note that the VV backscatter is generally larger than the HH backscatter; the variability arises due to the wind speed and direction. On the other hand, the X-band cross-pol backscatter is more-or-less hidden in the instrument noise floor. Although the X-band cross-pol backscatter could be exploitable for wind speed, which is the case for C-band cross-pol backscatter [6], these measurements made using TerraSAR-X do not have adequate signal-to-noise ratio to warrant further investigation here.

Figure 11 shows plots of the X-band co-pol and cross-pol backscatters as a function of the *in situ*-observed wind speed. Again, the instrument noise floor is plotted for each observation. The X-band co-pol data show the expected upward trend with increasing wind speed; the variability arises due to the incidence angle and wind direction.

Wind speed retrieval was carried out for X-band co-pol data using the XMOD GMF, as shown in Figure 12. The *in situ*-observed wind direction, φ, and the image orientation were used along with the XMOD GMF (for VV polarization) and a co-pol ratio (for HH polarization). The observed RMS errors are: X-band VV, 1.37 m/s; X-band HH, 1.84 m/s. These results are comparable to or better than previous TerraSAR-X wind retrieval results that had an RMS error of 2.50 m/s for X-band VV polarization data in comparison to QuikSCAT winds [1]. This indicates that the XMOD GMF is a viable means of modelling the expected ocean surface backscatter at X-band for both VV and HH polarizations.

a)

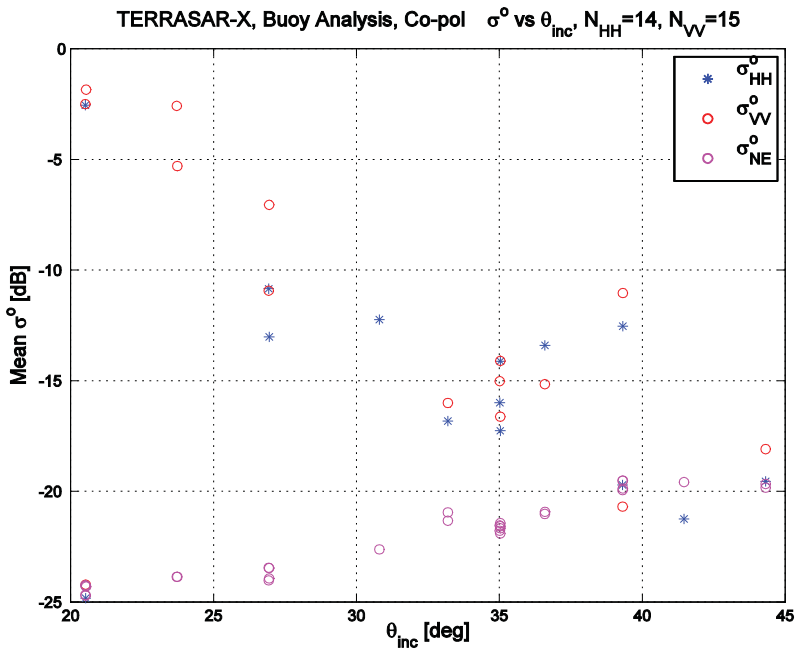

b)

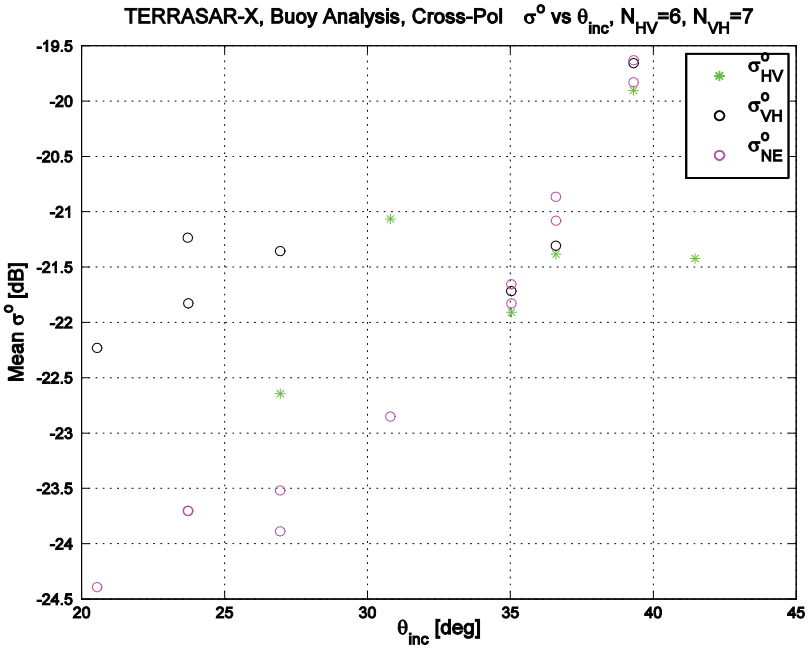

Figure 10: X-band sigma-naught versus incidence angle for: a) co-pol; and b) cross-pol.

a)

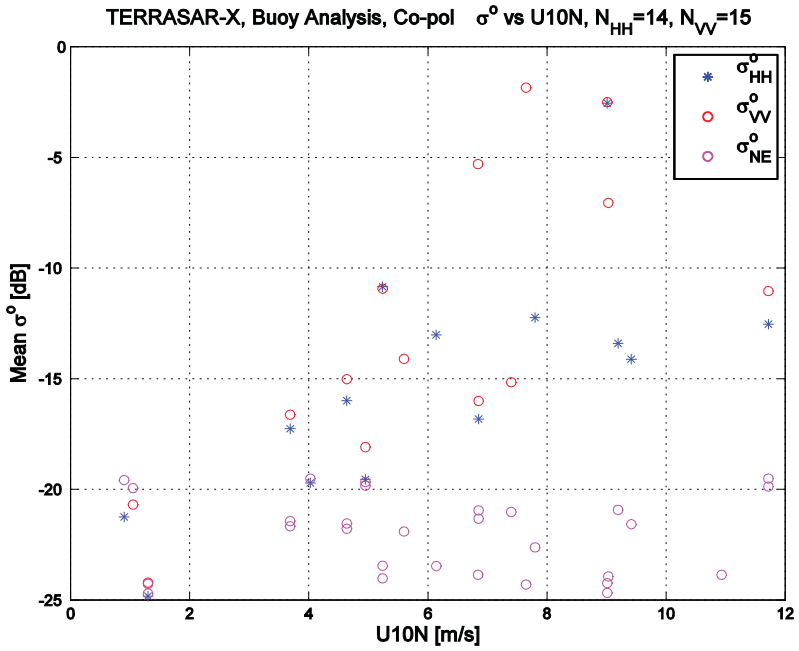

b)

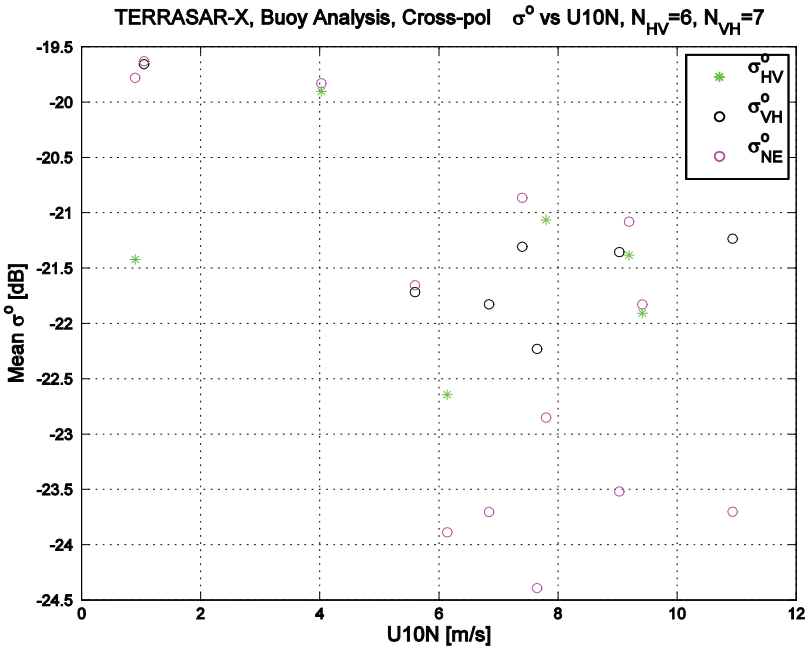

Figure 11: X-band sigma-naught versus wind speed for: a) co-pol; and b) cross-pol.

a)

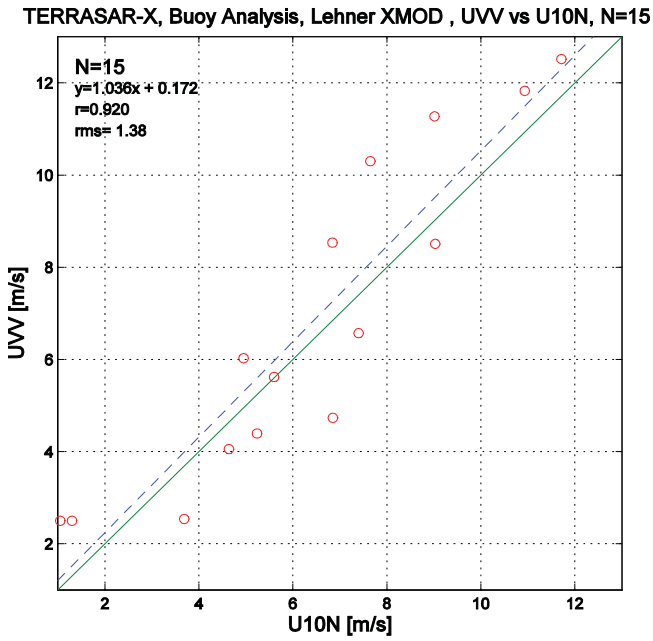

b)

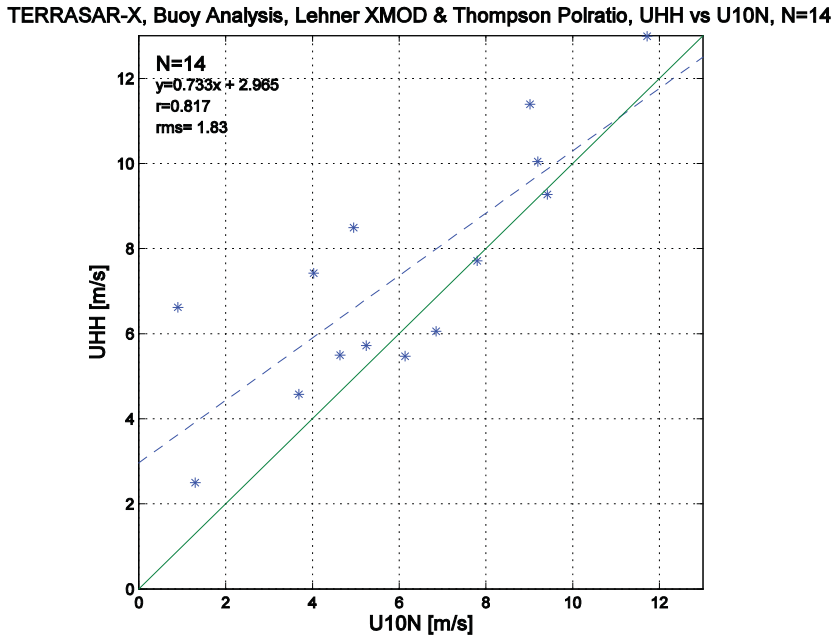

Figure 12: SAR-retrieved wind speed versus in situ-observed wind speed for: a) X-band VV polarization; and b) X-band HH polarization.

4 X-band ship detectability

Based upon the X-band ship RCS model developed in Section 2 and the XMOD GMF that was validated in Section 3, a C-band SAR Ship Detectability Performance Tool [5] has been extended to support X-band instruments. Details of the model and caveats associated with its use have been discussed at length elsewhere [5]. One of the main issues is that the X-band ship RCS model has been developed for rather large ship targets only; this modelling is intended to address the detectability of small vessels, so it is necessary to use the developed model to extrapolate to smaller target sizes. Furthermore, the model isn't expected to apply to higher resolution TerraSAR-X modes. As such, the upgraded tool is more relevant to the TerraSAR-X ScanSAR modes, which provide useful swath coverage for wide area maritime surveillance.

The upgraded ship detectability tool (see Figure 13) has been used to estimate the minimum detectable ship length ($L_{\min}$) for several scenarios. The calculations are based upon the following fixed parameter choices:

- Wind speed of 12 m/s – this wind speed is a representative case that corresponds roughly to sea state 5, and is an operational upper limit in which ship detection is desirable. A lower wind speed would result in better ship detection performance
- Wind blowing towards the radar – towards and away from the radar are the worst ocean clutter cases. Choice of a different wind direction would result in better ship detection performance.
- K-distribution order parameter of 4 – this order parameter is a fairly pessimistic case, but is consistent with the values estimated from single-look TerraSAR-X data (see Figure 9). A larger order parameter would result in better ship detection performance.
- Probability of false alarm of $2.5(10)^{-9}$ – this probability of false alarm is rather low. A higher false alarm rate permits the detection of smaller ships.
- Probability of detection of 0.9 – this probability of detection represents the performance of a useful ship detection system.
- Ship RCS margin of 3 dB – this parameter accounts for loss of target contrast due to the sampling grid, target defocus, target smearing, *etc*.
- HH polarization – use of HH polarization allows the detection of smaller ships than VV polarization since the clutter level is lower. X-band cross-pol ship detectability modelling has not been addressed due to the lack of a model to describe the X-band cross-pol clutter.

The new tool has been used to compare the ship detection performance at C-band and X-band for two generic beam modes that are similar to the available TerraSAR-X ScanSAR beam modes. The four-beam ScanSAR mode for radiometrically-enhanced products has a spatial resolution of roughly 18 m by 18 m (ground-range by azimuth) with 5 to 11 looks (from near to far swath edges). The six-beam ScanSAR mode for radiometrically-enhanced products has a spatial resolution of roughly 40 m by 40 with 6 to 8 looks. These cases were simulated at C-band and X-band for a fixed number of looks (5 and 7, respectively) and a noise floor of −22.5 dB, under the assumption that all else is held constant and equal, as plotted in Figure 14.

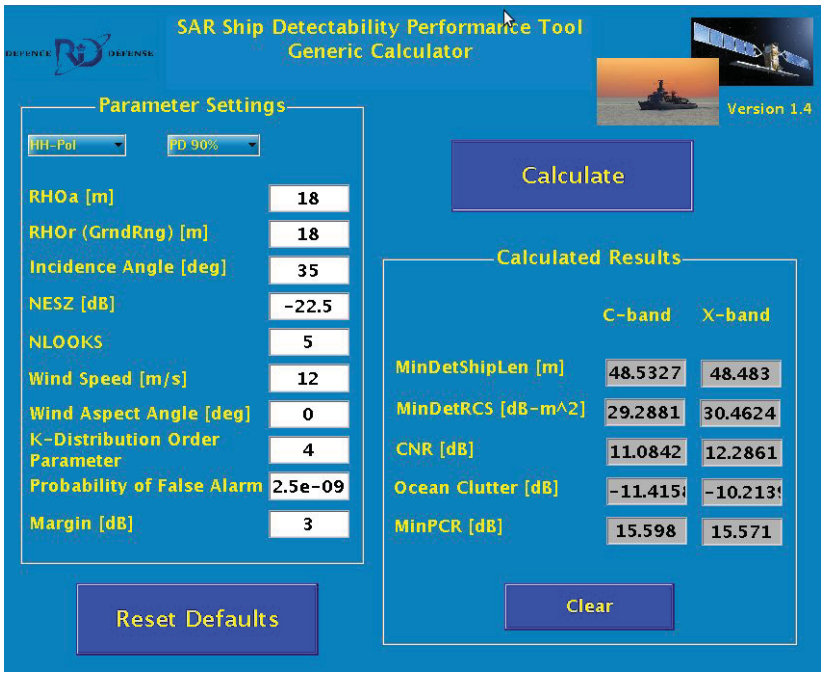

Figure 13: Screen-capture of the X-band SAR Ship Detectability Performance Tool, Generic Calculator.

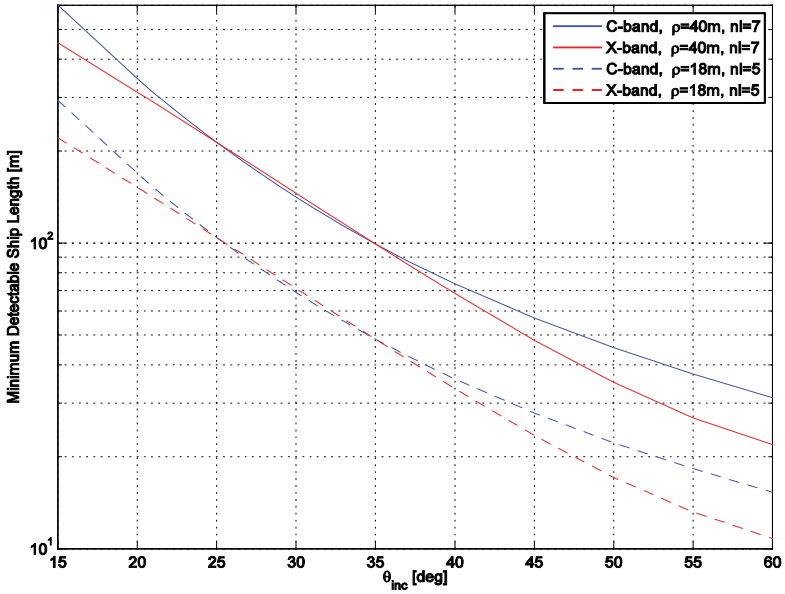

Figure 14: X-band and C-band minimum detectable ship length as a function of incidence angle.

It is apparent that X-band SAR, in general, is able to detect smaller vessels than C-band SAR. It is also interesting that the C-band and X-band ship detection performance are similar between 25° and 35° incidence angles. The differences in performance are attributed to the larger ship RCS at X-band and differences in the slope of the ocean clutter model with increasing incidence angle.

The X-band ship detection performance calculator could be used to predict the performance of other X-band SAR missions, and future systems such as the follow-on to the RADARSAT Constellation Mission.

5 Conclusions

A new semi-empirical model for X-band ship RCS, including uncertainties, has been developed using a database of validated ship signatures derived from TerraSAR-X images and shore-based AIS data. The model parameterizes the ship RCS in terms of the ship-length squared, and RCS variability is captured by percentile values of the observed ship RCS. The model was extended to handle the case of using the ship length estimated from the image itself, which broadens the range of possible RCS values. This type of model can be used to improve the performance of automatic ship detection systems by providing a range of RCS values that a ship signature must conform to, thereby providing a mechanism to reduce false alarms.

Furthermore, a recent X-band GMF, referred to as XMOD, was successfully validated using a set of TerraSAR-X images of operational Canadian meteorological buoys located off the east coast. RMS errors in comparing the SAR-derived and *in situ*-observed wind speeds were less than 2 m/s, for VV and HH polarization data.

The X-band ship RCS model and XMOD were integrated into a SAR Ship Detectability Performance Tool, permitting comparison of C-band and X-band SAR minimum detectable ship length. The tool is applicable to the coarser resolution ScanSAR modes of TerraSAR-X. It was shown that X-band offers as good as or better ship detectability (*i.e.*, a smaller minimum detectable ship length) than C-band, all else held equal. This is likely due to the ship having a higher RCS at X-band than at C-band.

Future improvements to the tool may be warranted. In particular, it is expected that better X-band ocean clutter models will be published in the near future. Furthermore, it would be desirable to include a model for the cross-pol clutter at X-band.

The upgraded ship detectability tool will prove to be useful in establishing the ship detection performance of future X-band SAR systems, which could include the follow-on to the RADARSAT Constellation Mission.

This page intentionally left blank.

References

[1] Ren, Y., Lehner, S., Brusch, S., Li, X., and He, M. (2012). An algorithm for the retrieval of sea surface wind fields using X-band TerraSAR-X data. *International Journal of Remote Sensing*, 33(23), 7310-7336. DOI: 10.1080/01431161.2012.685977

[2] Vachon, P.W., English, R.A., and Wolfe, J. (2007). Validation of RADARSAT-1 vessel signatures with AISLive data. *Canadian Journal of Remote Sensing*, 33(1), 20-26.

[3] Vachon, P.W., English, R.A., and Wolfe, J. (2007). Ship signatures in RADARSAT-1 ScanSAR Narrow B imagery: Analysis with AISLive data. DRDC Ottawa TM 2007-052, Defence R&D Canada – Ottawa.

[4] Vachon, P.W., and Wolfe, J. (2008). Validation of ship signatures in Envisat ASAR AP mode data using AISLive: Data acquisition, processing, and analysis results. DRDC Ottawa TM 2008-005, Defence R&D Canada – Ottawa.

[5] Vachon, P.W., and Wolfe, J. (2008). GMES Sentinel-1 Analysis of Marine Applications Potential (AMAP). DRDC Ottawa ECR 2008-218, Defence R&D Canada – Ottawa.

[6] Vachon, P.W. and Wolfe, J. (2011). C-band cross-polarization wind speed retrieval. *IEEE Geoscience and Remote Sensing Letters*, 8(3), 456-459. DOI: 10.1109/LGRS.2010.2085417

This page intentionally left blank.

Annex A Ocean wind observations

The ocean wind observations are summarized in Table A-1. In the table:

- Pol is the polarization;
- σ° is the observed ocean backscatter;
- $\sigma^\circ_{\mathrm{NE}}$ is the estimated instrument noise floor;
- θ_{inc} is the incidence angle at the buoy location;
- ΔT is the time difference between the SAR and the buoy measurements;
- $U^{10}_{\mathrm{neutral}}$ is the observed buoy wind speed converted to the equivalent neutral stability wind speed at ten metres height above the ocean surface;
- φ is the wind direction measured clockwise with respect to true North;
- U is the wind speed retrieved using XMOD or XMOD with a co-polarization ratio; and
- v is the estimated K-distribution order parameter.

Table A-1: X-band ocean wind observations.

	Buoy	Date and Time [UTC]	Pol	σ° [dB]	$\sigma^\circ_{\mathrm{NE}}$ [dB]	θ_{inc} [°]	ΔT [min]	$U^{10}_{\mathrm{neutral}}$ [m/s]	φ [°T]	U [m/s]	v
1	44138	2009-07-03 09:20	HH	−24.8	−24.7	20.5	8.3	1.3	147	2.5	100
2	44138	2009-07-03 09:20	VV	−24.2	−24.3	20.5	8.3	1.3	147	2.5	100
3	44138	2009-08-05 09:20	HH	−2.5	−24.7	20.5	8.2	8.3	211	11.4	2.8
4	44138	2009-08-05 09:20	VV	−2.5	−24.2	20.5	8.2	8.3	211	11.3	3.1
5	44138	2009-07-06 20:20	HH	−10.8	−23.5	26.9	14.7	5.0	225	5.7	1.4
6	44138	2009-07-06 20:20	VV	−10.9	−24.0	26.9	14.7	5.0	225	4.4	1.8
7	44138	2009-08-08 20:20	VH	−21.4	−23.5	27.0	14.7	8.4	249	-	74.0
8	44138	2009-08-08 20:20	VV	−7.1	−23.9	27.0	14.7	8.4	249	8.5	2.3
9	44138	2009-07-09 09:20	VH	−21.3	−20.9	36.6	16.8	7.1	52	-	100
10	44138	2009-07-09 09:20	VV	−15.2	−21.0	36.6	16.8	7.1	52	6.6	9.2
11	44138	2009-07-11 20:20	HH	−21.3	−19.6	41.5	23.2	0.9	205	6.6	100
12	44138	2009-07-11 20:20	HV	−21.4	−19.8	41.5	23.2	0.9	205	-	95.4
13	44138	2009-07-17 20:20	HH	−13.0	−23.5	26.9	14.7	5.7	174	5.5	2.8
14	44138	2009-07-17 20:20	HV	−22.6	−23.9	26.9	14.7	5.7	174	-	100
15	44138	2009-07-20 09:20	HH	−13.4	−20.9	36.6	16.8	8.5	254	10.0	3.5
16	44138	2009-07-20 09:20	HV	−21.4	−21.1	36.6	16.8	8.5	254	-	93.4
17	44138	2009-07-25 09:20	VH	−22.2	−24.4	20.5	8.3	7.2	92	-	100
18	44138	2009-07-25 09:20	VV	−1.8	−24.3	20.5	8.3	7.2	92	10.3	3.2
19	44139	2009-07-19 09:20	HH	−12.2	−22.6	30.8	0.4	7.8	236	7.7	5.4
20	44139	2009-07-19 09:20	HV	−21.1	−22.9	30.8	0.4	7.8	236	-	100
21	44139	2009-06-22 09:20	HH	−19.5	−19.7	44.3	8.2	4.9	102	8.5	51.4
22	44139	2009-06-22 09:20	VV	−18.1	−19.8	44.3	8.2	4.9	102	6.0	52.8
23	44139	2009-06-24 21:20	HH	−16.8	−21.0	33.2	28.1	6.8	180	6.1	4.7

	Buoy	Date and Time [UTC]	Pol	σ° [dB]	σ°_{NE} [dB]	θ_{inc} [°]	ΔT [min]	$U^{10}_{neutral}$ [m/s]	φ [°T]	U [m/s]	v
24	44139	2009-06-24 21:20	VV	−16.0	−21.3	33.2	28.1	6.8	180	4.7	6.3
25	44141	2009-08-01 21:20	HH	−12.5	−19.5	39.3	19.8	10.9	234	13.0	15.0
26	44141	2009-08-01 21:20	VV	−11.0	−19.9	39.3	19.8	10.9	234	12.5	8.8
27	44141	2009-07-05 21:20	VH	−21.2	−23.7	23.7	28.4	10.3	262	-	47.7
28	44141	2009-07-05 21:20	VV	−2.6	−23.9	23.7	28.4	10.3	262	11.8	2.4
29	44141	2009-07-08 09:20	VH	−21.7	−21.7	35.0	0.7	5.4	77	-	100
30	44141	2009-07-08 09:20	VV	−14.1	−21.9	35.0	0.7	5.4	77	5.6	8.7
31	44141	2009-08-10 09:20	HH	−16.0	−21.5	35.0	0.8	4.5	267	5.5	3.9
32	44141	2009-08-10 09:20	VV	−15.0	−21.8	35.0	0.8	4.5	267	4.1	5.1
33	44141	2009-07-10 21:20	VH	−19.7	−19.6	39.3	19.8	1.1	86	-	100
34	44141	2009-07-10 21:20	VV	−20.7	−19.9	39.3	19.8	1.1	86	2.5	100
35	44141	2009-07-16 21:20	VH	−21.8	−23.7	23.7	28.4	6.5	239	-	94.3
36	44141	2009-07-16 21:20	VV	−5.3	−23.9	23.7	28.4	6.5	239	8.5	1.8
37	44141	2009-07-19 09:20	HH	−14.1	−21.6	35.0	0.8	8.8	225	9.3	3.7
38	44141	2009-07-19 09:20	HV	−21.9	−21.8	35.0	0.8	8.8	225	-	100
39	44141	2009-08-21 09:20	HH	−17.3	−21.4	35.0	0.8	3.5	254	4.6	3.1
40	44141	2009-08-21 09:20	VV	−16.6	−21.7	35.0	0.8	3.5	254	2.5	3.8
41	44141	2009-07-21 21:20	HH	−19.7	−19.5	39.3	19.8	3.8	181	7.4	100
42	44141	2009-07-21 21:20	HV	−19.9	−19.8	39.3	19.8	3.8	181	-	100

List of acronyms

AIS	Automatic Identification System
ASAR	Advance SAR (instrument on Envisat)
CPDF	Cumulative Probability Density Function
DLR	Deutsches Zentrum für Luft- und Raumfahrt e.V. (German Aerospace Center)
DOI	Digital Object Identifier
DRDC	Defence R&D Canada
ESL	Estimated Ship Length
GMF	Geophysical Model Function
HH	Horizontal transmit polarization, Horizontal receive polarization
HV	Horizontal transmit polarization, Vertical receive polarization
ISR	Internet Ships Register
ISR	Intelligence, Surveillance, and Reconnaissance
MSSIS	Maritime Safety and Security Information System
NE	Normalized Error
RCS	Radar Cross Section
RMS	Root Mean Square
SAR	Synthetic Aperture Radar
STD	Standard Deviation
VH	Vertical transmit polarization, Horizontal receive polarization
VHF	Very High Frequency
VSL	Validated Ship Length
VV	Vertical transmit polarization, Vertical receive polarization
XMOD	X-band Model

This page intentionally left blank.

DOCUMENT CONTROL DATA

(Security classification of title, body of abstract and indexing annotation must be entered when the overall document is classified)

1. ORIGINATOR (The name and address of the organization preparing the document. Organizations for whom the document was prepared, e.g. Centre sponsoring a contractor's report, or tasking agency, are entered in section 8.)

Defence R&D Canada – Ottawa3701 Carling AvenueOttawa, Ontario K1A 0Z4

2. SECURITY CLASSIFICATION (Overall security classification of the document including special warning terms if applicable.)

UNCLASSIFIED
(NON-CONTROLLED GOODS)
DMC A
REVIEW: GCEC APRIL 2011

3. TITLE (The complete document title as indicated on the title page. Its classification should be indicated by the appropriate abbreviation (S, C or U) in parentheses after the title.)

Development of an X-band SAR ship detectability model: Analysis of TerraSAR-X ocean imagery

4. AUTHORS (last name, followed by initials – ranks, titles, etc. not to be used)

Vachon, P.W.; English, R.; Sandirasegaram, N.; Wolfe, J.

5. DATE OF PUBLICATION (Month and year of publication of document.)	6a. NO. OF PAGES (Total containing information, including Annexes, Appendices, etc.)	6b. NO. OF REFS (Total cited in document.)
December 2013	38	6

7. DESCRIPTIVE NOTES (The category of the document, e.g. technical report, technical note or memorandum. If appropriate, enter the type of report, e.g. interim, progress, summary, annual or final. Give the inclusive dates when a specific reporting period is covered.)

Technical Memorandum

8. SPONSORING ACTIVITY (The name of the department project office or laboratory sponsoring the research and development – include address.)

Defence R&D Canada – Ottawa3701 Carling AvenueOttawa, Ontario K1A 0Z4

9a. PROJECT OR GRANT NO. (If appropriate, the applicable research and development project or grant number under which the document was written. Please specify whether project or grant.)	9b. CONTRACT NO. (If appropriate, the applicable number under which the document was written.)
15ea02	

10a. ORIGINATOR'S DOCUMENT NUMBER (The official document number by which the document is identified by the originating activity. This number must be unique to this document.)	10b. OTHER DOCUMENT NO(s). (Any other numbers which may be assigned this document either by the originator or by the sponsor.)
DRDC Ottawa TM 2013-120	

11. DOCUMENT AVAILABILITY (Any limitations on further dissemination of the document, other than those imposed by security classification.)

Unlimited

12. DOCUMENT ANNOUNCEMENT (Any limitation to the bibliographic announcement of this document. This will normally correspond to the Document Availability (11). However, where further distribution (beyond the audience specified in (11) is possible, a wider announcement audience may be selected.))

Unlimited

13. ABSTRACT (A brief and factual summary of the document. It may also appear elsewhere in the body of the document itself. It is highly desirable that the abstract of classified documents be unclassified. Each paragraph of the abstract shall begin with an indication of the security classification of the information in the paragraph (unless the document itself is unclassified) represented as (S), (C), (R), or (U). It is not necessary to include here abstracts in both official languages unless the text is bilingual.)

A C-band SAR Ship Detectability Performance Tool has been extended to X-band synthetic aperture radar (SAR) by analyzing TerraSAR-X ocean imagery. First, a database of validated X-band SAR ship signatures was developed using coastal-received Automatic Identification System (AIS) data over the Strait of Gibraltar. The database was used to derive a semi-empirical model for the ship radar cross section (RCS) and its variability. Second, X-band SAR imagery of meteorological buoys has provided a set of X-band ocean backscatter measurements for known wind conditions. These measurements have been used to validate a model that relates X-band ocean backscatter to wind speed. The upgraded X-band SAR Ship Detectability Performance Tool can be used to predict the ship detection performance of existing and future X-band SAR missions, which could include the follow-on to the RADARSAT Constellation Mission.

14. KEYWORDS, DESCRIPTORS or IDENTIFIERS (Technically meaningful terms or short phrases that characterize a document and could be helpful in cataloguing the document. They should be selected so that no security classification is required. Identifiers, such as equipment model designation, trade name, military project code name, geographic location may also be included. If possible keywords should be selected from a published thesaurus, e.g. Thesaurus of Engineering and Scientific Terms (TEST) and that thesaurus identified. If it is not possible to select indexing terms which are Unclassified, the classification of each should be indicated as with the title.)

synthetic aperture radar; SAR; TerraSAR-X; X-band; ship detection; Automatic Identification System; AIS; Maritime Safety and Security Information System; MSSIS